Peer-Reviewed Technical Communication

Motion Analysis of an Autonomous Underwater Vehicle Tethered With an Optical Fiber for Real-Time Surveillance

Shuangshuang Fan, Kamchau Chan, and Christopher K. H. Chin

***Abstract*—Autonomous underwater vehicles (AUVs) are playing an increasingly important role in ocean exploration. In some applications, an AUV can be tethered by a communication cable, such as an optical fiber, for real-time surveillance. This article focuses on the motion analysis of the AUV and cable coupling system to investigate the interaction between AUV and cable dynamic behaviors, especially under the current disturbance in the dynamic ocean environment. The dynamic equations of the coupled AUV and cable are derived using the well-known finite difference method and solved using the advanced trust-region method in MATLAB. The model-based simulation scheme is presented and further verified by comparing the simulation results with the validated ones published in the existing literature. The motion cases when the tethered vehicle maneuvers in a variety of motion modes and current scenarios are studied to conduct a systematic motion analysis. Both the variation in the cable tension at the towpoint and the configuration of the cable in the water are investigated. Based on the understanding of the cable and current effects on AUV motion, this article further explores the antitwining maneuvering strategy for the cable-tethered AUV moving in currents. The findings in this work can provide theoretical guidance for the safe operation of the AUV and cable coupling system in the field.**

***Index Terms*—Antitwining maneuvering strategy, autonomous underwater vehicles (AUVs), cable dynamics, finite difference method (FDM), ocean current effects.**

1. Introduction

AUTONOMOUS underwater vehicles (AUVs) are unmanned underwater robots that are capable of conducting various preprogrammed missions ranging from seabed survey, coastal mapping, and environmental monitoring for scientific and industrial purposes to antisubmarine warfare for defense purposes [1]–[5]. Over the past decades, AUVs have proven to be effective and efficient in performing the tasks in dangerous, distant, and dynamic ocean environments.

The major task of an AUV is to collect information from the underwater environment and send the data back to the onshore control center, for which the reliable data transmission is required. However, according to the current available technology, underwater communication has always been an important challenge in the field. In general, there are three kinds of approaches widely applied for underwater communication, which are through acoustic wave, blue light, and optical fiber. Due to the different communication mechanisms, each method has both its pros and cons. Acoustic signal can be transmitted over 10 km; however, it has the disadvantage of low transmission rate and being detected easily. Besides, the performance of the acoustic sonar relies on the propagation environment heavily [6], [7]. Blue light can provide higher data transmission rate than the acoustic wave; however, its communication distance is very limited, only within 100 m [8], [9]. Thus, to have real-time and reliable underwater communication through large range, using an optical fiber could be a better solution for the real-time surveillance mission of an AUV [10], [11]. In this case, there will be challenges in terms of AUV operation to avoid twining between the vehicle and the tethered cable, especially in high dynamic ocean environment with wave and current disturbances.

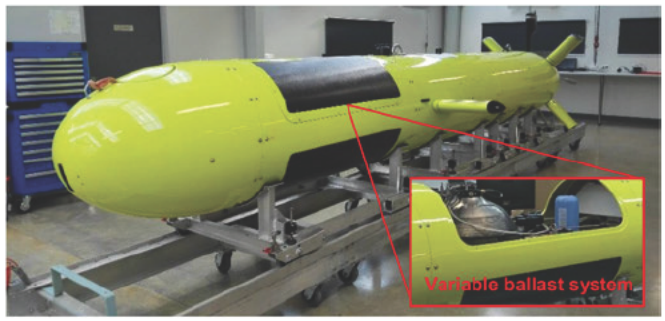

Fig. 1. AMC Explorer AUV with a variable ballast system.

Australian Maritime College (AMC), University of Tasmania, Launceston, TAS, Australia, owns an Explorer class AUV, which was built by a Canadian company, International Submarine Engineering, Port Coquitlam, BC, Canada, and can reach a depth of 5000 m [12]. The AMC Explorer AUV is able to act as a stationary and relocatable platform due to its unique configuration (see Fig. 1). With a variable ballast system, the vehicle could land on the seafloor for long-term surveillance of the water column above it. For rapid response purpose, the AUV will be tethered with an optical fiber for real-time communication. In this case, special attention is required to be paid to the vehicle's manoeuvering behavior and motion control strategy, to investigate the cable effects and avoid the twining issue.

The motion of a long flexible buoyant cable in water is very complex, in addition to the nonlinear dynamic motion of the AUV, which makes the motion analysis of the coupled AUV and cable system even more challenging. There are several methods with different assumptions and

Manuscript received March 31, 2019; revised October 30, 2019 and February 27, 2020; accepted April 2, 2020. This work was supported by the Strategic Priority Research Program of the Chinese Academy of Sciences under Grant XDA22000000. *(Corresponding author: Shuangshuang Fan.)*

Associate Editor: B. Englot.

Shuangshuang Fan is with the School of Marine Sciences, Sun Yat-sen University, Zhuhai 519082, China, and also with the Southern Laboratory of Ocean Science and Engineering, Zhuhai 519000, China (e-mail: fanshsh6@mail.sysu.edu.cn).

Kamchau Chan and Christopher K. H. Chin are with the Australian Maritime College, University of Tasmania, Launceston, TAS 7250, Australia (e-mail: kamchauc@utas.edu.au; c.chin@utas.edu.au).

Digital Object Identifier 10.1109/JOE.2020.2986876

considerations for the motion study of a cable-tethered vehicle system, which include analytical method, experimental method, lumped mass method (LMM), catenary method, and finite difference method (FDM). The analytical method was initially studied by Casarella and Parsons; however, the application of this method is very limited as it can only be used to solve the simple problem when the studied system is at rest [13]. Experimental method can be considered as the most reliable method to predict the dynamic behavior of the cable-tethered vehicle system [14], [15]; however, the experimental method is very time consuming and costly, and the conduction of the experiment in the field has many limitations and challenges. The LMM considers the cable as a discretized system consisting of microunits connected by an elastic nonmass spring [16], [17]. In this chain-connected spring system, although all the forces are considered for each node, the bending stiffness of the cable is neglected, which is less realistic. Mai *et al.* presented a governing dynamic equation for the combined motion of the vehicle and cable system based on the catenary equation and applied the shooting method to solve the two-point boundary problem of the catenary equation [11]. In this catenary method, the two ends of the cable are fixed so that the length of the deployed cable is also fixed; however, it is not applicable to the case in our study, for which the cable is deployed by a drum on the deck of the support ship with increased length and negligible tension when it is pulled by the vehicle.

In recent years, the FDM has become more popular. It assumes the cable as a long, thin, flexible, and circular cylinder, which is built up by finite elements. In this way, the motion of each element can be modeled with all acting forces considered [18]. Due to these reasonable considerations, this method has been referenced for cable modeling in many studies, and the proposed FDM has been extensively utilized and approved in different applications. Milinazzo *et al.* introduced a set of equations to calculate the initial conditions of the cable, which makes it more stable and efficient to solve the motion equations [19]. For a typical towed cable system, where the length of the cable is fixed, numerical solutions of the equations can be obtained by the proposed FDMs [18], [19]. However, these numerical schemes cannot be applied to our mentioned situation directly due to the varied cable length. Feng and Allen extended the numerical scheme developed by Milinazzo *et al.* and evaluated the effects of the communication cable with nonfixed length on the Subzero II AUV [10]. In Feng and Allen's work, the least squares solution was adopted to solve the nonlinear finite differential equations. As the calculation capability of MATLAB Optimization Toolbox improves, there are more advanced solving methods that can provide individual benefits, such as higher efficiency, lower memory requirement, and higher accuracy.

In this article, we will apply the well-known FDM to conduct motion analysis of the AUV and cable coupling system. To solve the nonlinear differential equations, different iteration methods are applied to the respective AUV and cable dynamic equations due to their different dynamic characteristics. Usually, the Runge–Kutta method is well known to solve the differential equations of AUV dynamics, whereas either the trust-region (TR) method, TR dogleg (TRD) method, or the Newton–Raphson (NR) method could be used to solve the partial differential equations of cable dynamics. TR, TRD, and NR methods are well developed advanced equation solving algorithms in MATLAB nowadays [20]. They can provide more accurate results than the least squares method, as is used in Feng and Allen's work; however, they are less considered in the existing relevant research so far, to the best of our knowledge.

Among these three methods, the TRD method has the fastest computing speed, followed by the TR and NR methods. In general, the TR method could provide more accurate results than the other two methods;

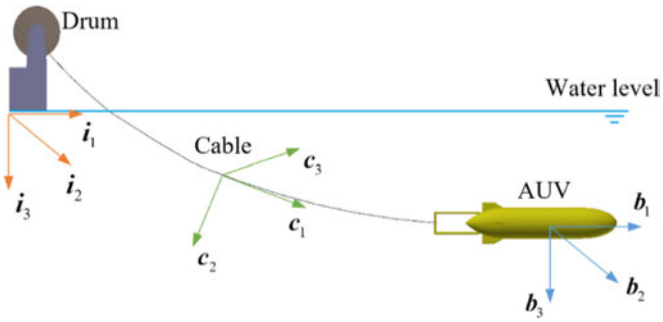

Fig. 2. Definition of coordinate systems.

however, this method requires large amount of computation resource to solve the equations. The NR method is a kind of primeval iteration algorithm. Although its computing speed is slower than that of the other two methods, it requires less memory during its computation, making its performance better when dealing with complicated problems. As a result, users should choose their suitable method with the given problem. The methods mentioned above would require a Jacobian matrix to solve the partial differential equations, where the Jacobian matrix could be calculated by using the built-in function of MATLAB program [20]. In this article, the TR method is adopted to solve the nonlinear finite differential equations in all the case studies to achieve more accurate results.

By using the FDM numerical scheme, this article will focus on the investigation of not only the cable effects on AUV operation but also the environmental impact on the coupled AUV and cable system, such as the ocean current disturbances. The cases when the vehicle manoeuvers in a variety of motion modes and current scenarios will be studied to conduct a systematic motion analysis. Based on this, antitwining maneuvering strategies will be proposed to make the tethered AUV system operate safely in the harsh ocean environment.

The rest of this article is organized as follows. Section II presents the dynamic model of the coupled AUV and cable system. In Section III, we introduce and verify our model-based simulation scheme. The motion analysis of the coupled system moving in a series of scenarios is conducted by numerical simulation in Section IV, whereas the simulation results are further discussed in Section V. Section VI summarizes the main contributions and describes some additional avenues for continuing research.

II. Dynamics Modeling of the AUV and Cable Coupling System

As a complex dynamics coupling system, the mathematical model of the cable-tethered AUV is composed of two parts: kinematic model and dynamic model. Its modeling method will be presented respectively in details in this section.

A. Kinematic Model

1) AUV Kinematic Model: First, an inertially fixed frame $\{\boldsymbol{i}_1, \boldsymbol{i}_2, \boldsymbol{i}_3\}$ and a body-fixed reference frame $\{\boldsymbol{b}_1, \boldsymbol{b}_2, \boldsymbol{b}_3\}$ are defined to derive the motion equations of an AUV, as is shown in Fig. 2. Each of the reference frames consists of a triad of orthogonal vectors defined according to the right-hand rule. The origin of the inertial frame is fixed at the drum, whereas the origin of the body frame is fixed at the buoyancy center of the vehicle. The orientation of the body frame is given by the

rotation matrix $\boldsymbol{R}$, which is parameterized by Euler angles, that is the roll angle ϕ, the pitch angle θ, and the yaw angle ψ. Let $\boldsymbol{e}_i$ represent the standard basis vector for $\mathbb{R}^3$, $i \in 1, 2, 3$, and let the character $\hat{\cdot}$ denote the 3×3 skew-symmetric matrix operator satisfying $\hat{\boldsymbol{a}}\boldsymbol{b} = \boldsymbol{a} \times \boldsymbol{b}$ for vectors $\boldsymbol{a}$ and $\boldsymbol{b}$, where the symbol $\times$ denotes the cross product of two vectors. Then, in terms of conventional Euler angles, we have

$$\boldsymbol{R}(\phi, \theta, \psi) = e^{\hat{\boldsymbol{e}}_3 \psi} e^{\hat{\boldsymbol{e}}_2 \theta} e^{\hat{\boldsymbol{e}}_1 \phi}$$

where $\boldsymbol{R}(\phi, \theta, \psi)$ can be used to indicate the relationship between the vectors expressed in inertial and body frames

$$\boldsymbol{X} = \boldsymbol{R}(\phi, \theta, \psi)\boldsymbol{x} \tag{1}$$

where $\boldsymbol{x} = [x, y, z]^T$ defines a position vector expressed in the body frame, and $\boldsymbol{X} = [X, Y, Z]^T$ denotes a position vector expressed in the inertial frame.

Let $\boldsymbol{v} = [u, v, w]^T$ and $\boldsymbol{\omega} = [p, q, r]^T$ represent the respective translational and rotational velocities of the vehicle with respect to the inertial frame but expressed in the body frame. The kinematic equations of the vehicle are

$$\dot{\boldsymbol{X}}_v = \boldsymbol{R}(\phi, \theta, \psi)\boldsymbol{v} \tag{2}$$

$$\dot{\boldsymbol{R}} = \boldsymbol{R}(\phi, \theta, \psi)\hat{\boldsymbol{\omega}} \tag{3}$$

where $\boldsymbol{X}_v = [X_v, Y_v, Z_v]^T$ denotes the position vector of the vehicle, expressed in the inertial frame. Note that $\boldsymbol{v}$ represents the absolute velocity of the vehicle with respect to the inertial frame, but expressed in the body frame. It is the sum of the relative velocity of the vehicle with respect to the water $\boldsymbol{v}_r$ and the velocity of the ocean current $\boldsymbol{v}_c$. Both $\boldsymbol{v}_r$ and $\boldsymbol{v}_c$ are expressed in the body frame.

2) Cable Kinematic Model: A cable-fixed reference frame $\{\boldsymbol{c}_1, \boldsymbol{c}_2, \boldsymbol{c}_3\}$ is defined along the cable to describe the motion of the cable (see Fig. 2). The cable frames are located at points along the cable with $\boldsymbol{c}_1$ tangent to the cable in the direction of increasing arc length from the drum-side towpoint, and $\boldsymbol{c}_3$ in the plane of $\{\boldsymbol{i}_1, \boldsymbol{i}_2\}$. The orientation of the cable frame is given by the rotation matrix $\boldsymbol{W}$, which maps free vectors from the inertial frame to the cable frame. $\boldsymbol{W}$ is parameterized by two rotation angles: α and β, where a rotation through angle $(-\alpha)$ about the $\boldsymbol{i}_3$ axis to bring the $\boldsymbol{i}_1$ axis into the plane of $\{\boldsymbol{c}_1, \boldsymbol{c}_2\}$, rotation about the new $\boldsymbol{i}_1$ axis through $(-\pi/2)$ to bring $\boldsymbol{i}_3$ into coincidence with $\boldsymbol{c}_3$, and rotation about $\boldsymbol{c}_3$ through β to bring $\boldsymbol{i}_1$ and $\boldsymbol{i}_2$ into coincidence with $\boldsymbol{c}_1$ and $\boldsymbol{c}_2$. The signs have been chosen to permit agreement with [18].

Let $\boldsymbol{c} = [t, n, b]^T$ represent a vector (the position of a point along the cable) defined in the cable frame. With the rotation matrix $\boldsymbol{W}$, the relationship between the vectors expressed in the cable frame and the inertial frame can be expressed as follows [18], [19]:

$$\boldsymbol{c} = \boldsymbol{W}(\alpha, \beta)\boldsymbol{X} \tag{4}$$

where

$$\boldsymbol{W}(\alpha, \beta) = \begin{bmatrix} \cos\alpha\cos\beta & -\sin\alpha\cos\beta & -\sin\beta \\ -\cos\alpha\sin\beta & \sin\alpha\sin\beta & -\cos\beta \\ \sin\alpha & \cos\alpha & 0 \end{bmatrix}.$$

According to (1) and (4), the relationship between the vectors expressed in the body and cable frames can be written in terms of $\boldsymbol{R}(\phi, \theta, \psi)$ and $\boldsymbol{W}(\alpha, \beta)$

$$\boldsymbol{c} = \boldsymbol{W}(\alpha, \beta)\boldsymbol{R}(\phi, \theta, \psi)\boldsymbol{x}. \tag{5}$$

Let $\boldsymbol{V}_c = [V_t, V_n, V_b]^T$ represent the velocity vector of a point along the cable, which is expressed in the cable frame. The kinematic equation of the cable can be written as

$$\dot{\boldsymbol{X}}_c = \boldsymbol{W}^T(\alpha, \beta)\boldsymbol{V}_c \tag{6}$$

where $\boldsymbol{X}_c$ denotes the position vector of a point along the cable, expressed in the inertial frame.

B. Dynamic Model

In this section, the dynamic model of the AUV and cable coupling system will be derived separately. Then, the interaction between AUV and cable dynamic behaviors will be further identified.

1) AUV Dynamic Model: According to [21], the following equations show the dynamic equations of an AUV expressed in body-fixed frame:

$$m[\dot{u} - vr + wq - x_g(q^2 + r^2) + y_g(pq - \dot{r}) + z_g(pr + \dot{q})] = f_1 \tag{7}$$

$$m[\dot{v} - wp + ur - y_g(p^2 + r^2) + z_g(qr - \dot{p}) + x_g(qp + \dot{r})] = f_2 \tag{8}$$

$$m[\dot{w} - uq + vp - z_g(p^2 + q^2) + x_g(rp - \dot{q}) + y_g(rq + \dot{p})] = f_3 \tag{9}$$

$$I_1\dot{p} + (I_3 - I_2)qr - (\dot{r} + pq)I_{31} + (r^2 - q^2) I_{23} + m[y_g(\dot{w} - uq + vp) - z_g(\dot{v} - wp + ur)] = m_1 \tag{10}$$

$$I_2\dot{q} + (I_1 - I_3)rp - (\dot{p} + qr)I_{12} + (p^2 - r^2)I_{31} + (qp - \dot{r}) I_{23} + m[z_g(\dot{u} - vr + wq) - x_g(\dot{w} - uq + vp)] = m_2 \tag{11}$$

$$I_3\dot{r} + (I_2 - I_1)pq - (\dot{q} + rp)I_{23} + (q^2 - p^2)I_{12} + (rq - \dot{p}) I_{31} + m[x_g(\dot{v} - wp + ur) - y_g(\dot{u} - vr + wq)] = m_3 \tag{12}$$

where m denotes the mass of the vehicle. The center of gravity of the vehicle is located at $\boldsymbol{x}_g = [x_g, y_g, z_g]^T$. I_1, I_2, and I_3 are the moments of inertia of the vehicle with respect to each axis of body frame, whereas I_{12}, I_{23}, and I_{31} are the products of inertia. $\boldsymbol{f} = [f_1, f_2, f_3]^T$ and $\boldsymbol{m} = [m_1, m_2, m_3]^T$are the external forces and moments acting on the vehicle respectively, which are those due to the following:

1) gravity and buoyancy ($\boldsymbol{f}_{g/b}$ and $\boldsymbol{m}_{g/b}$);
2) hydrodynamic effects ($\boldsymbol{f}_v$ and $\boldsymbol{m}_v$);
3) ocean current effects ($\boldsymbol{f}_{\mathrm{cur}}$ and $\boldsymbol{m}_{\mathrm{cur}}$);
4) propulsion and control ($\boldsymbol{f}_{\mathrm{ctrl}}$ and $\boldsymbol{m}_{\mathrm{ctrl}}$);
5) cable effects ($\boldsymbol{f}_{\mathrm{cab}}$ and $\boldsymbol{m}_{\mathrm{cab}}$).

Since there are well developed studies on the modeling methods of the above each force and moment component in AUV dynamics [22]–[25], we save the details in this article. Thus, the complete external force and moment can be expressed as follows:

$$\boldsymbol{f} = \boldsymbol{f}_{g/b} + \boldsymbol{f}_v + \boldsymbol{f}_{\mathrm{cur}} + \boldsymbol{f}_{\mathrm{ctrl}} + \boldsymbol{f}_{\mathrm{cab}} \tag{13}$$

$$\boldsymbol{m} = \boldsymbol{m}_{g/b} + \boldsymbol{m}_v + \boldsymbol{m}_{\mathrm{cur}} + \boldsymbol{m}_{\mathrm{ctrl}} + \boldsymbol{m}_{\mathrm{cab}}. \tag{14}$$

2) Cable Dynamic Model: When modeling the cable dynamics, the cable is divided into finite small segments with equal length. The motion states of each segment of the cable can be represented by defining the following vector:

$$\boldsymbol{y}(s, t) = (T, V_t, V_n, V_b, \alpha, \beta)^T \tag{15}$$

where s and t denote the cable segments measured from the towpoint at vehicle side and the time instant, respectively, T is the tension acting along the cable, and $\boldsymbol{V}_c = [V_t, V_n, V_b]^T$represents the absolute velocity vector of one

segment along the cable, which is expressed in the cable frame. The dynamic model of the whole cable can be expressed in the form of following partial differential equation [18]:

$$\mathbf{M}\frac{\partial y}{\partial s} = \mathbf{N}\frac{\partial y}{\partial t} + \boldsymbol{q} \tag{16}$$

where we have the equation details shown at the bottom of the page.

Here, ρ is the fluid density, m_c denotes the mass per unit length of the cable, A is the cross-sectional area of the cable, m_{cv} means the virtual mass per unit length, which is equal to $m_c + \rho A$, g is the gravitational acceleration, w_c represents the immersed weight per unit length, which is equal to $(m_c - \rho A)g$, e is equal to $1/EA$, where E is Young's modulus, C_t and C_n are the tangential and normal drag coefficients, respectively, d is the diameter of the cable, $\boldsymbol{J} = [J_t, J_n, J_b]^T$ is the velocity of the ocean current, expressed in the cable frame, and $\boldsymbol{U} = [U_t, U_n, U_b]^T$ denotes the cable velocity relative to the ocean current, that is $\boldsymbol{U} = \boldsymbol{V}_c - \boldsymbol{J}$. From the above definition of each parameter involved in the vector $\boldsymbol{q}$, we can see that the external and internal forces and moments acting on the cable include: the gravity and buoyancy of the cable, elastic effects along the cable, hydrodynamic drag, current induced forces, and moments.

The following equations, developed by Ablow and Schechter [18], are used to represent the cable effects on AUV dynamics, where the cable-induced forces and moments are expressed in the vehicle body frame as follows:

$$\boldsymbol{f}_{\text{cab}}(t) = \begin{bmatrix} f_{c1} \\ f_{c2} \\ f_{c3} \end{bmatrix} = \boldsymbol{R}(\phi,\theta,\psi)^T \left\{ -\boldsymbol{W}(\alpha,\beta)^T \begin{bmatrix} T \\ 0 \\ 0 \end{bmatrix} \right\} \tag{17}$$

$$\boldsymbol{m}_{\text{cab}}(t) = \begin{bmatrix} m_{c1} \\ m_{c2} \\ m_{c3} \end{bmatrix} = \begin{bmatrix} y_c f_{c3} - z_c f_{c2} \\ z_c f_{c1} - x_c f_{c3} \\ x_c f_{c2} - y_c f_{c1} \end{bmatrix} \tag{18}$$

where $\boldsymbol{r}_c = [x_c, y_c, z_c]^T$ denotes the location of the towpoint at the vehicle side, expressed in the vehicle body frame. Note that cable caused forces and moments acting on the vehicle varies with the time instant. This is because the deployed cable length changes with time when the AUV towing the cable moves in the water.

Six boundary conditions are defined to specify the solution of the governing equations (16). The immersed part of the cable has two ends: the vehicle-towed end and the drum-released end. The vehicle-towed end is fixed at the tail of the vehicle, whereas the drum-released end is located at the drum at the deck of the ship, which deploys the cable into the water during the pull of the vehicle. The vehicle-towed end shares the same vehicle velocity with the cable at the towpoint so that the boundary conditions of this end can be defined in the cable frame as [10]

$$\begin{aligned} \boldsymbol{V}_c(0,t) &= [V_t(0,t), V_n(0,t), V_b(0,t)]^T \\ &= \boldsymbol{W}(\alpha,\beta)\boldsymbol{R}(\phi,\theta,\psi)(\boldsymbol{v} + \boldsymbol{\omega} \times \boldsymbol{r}_t) \end{aligned} \tag{19}$$

where $\boldsymbol{r}_t = [x_t, y_t, z_t]^T$ denotes the position of the towpoint in the vehicle body frame. In (19), the term $\boldsymbol{v} + \boldsymbol{\omega} \times \boldsymbol{r}_t$ means the velocity of the towpoint expressed in the vehicle body frame.

At the drum end of the cable, since a drum is applied to release the cable constantly along the tangent of the cable, we assume there is no tension force generated during this process. Thus, the boundary conditions at the drum-released end are

$$T(S_t, t) = 0 \tag{20}$$

$$V_n(S_t, t) = 0 \tag{21}$$

$$V_b(S_t, t) = 0 \tag{22}$$

where S_t is the total arc length of the deployed cable at time *t*.

Combining the kinematic equations (2), (3), and (6), with the dynamic equations (7)–(12) and (16), one obtains a complete dynamic model for the AUV and cable coupling system. Note that different from Feng and Allen's work in [10], here we consider the current effects on both the AUV and the cable dynamics. In the following study, the model-based simulation is conducted to predict the motion of the coupled system, especially under the disturbance of ocean currents.

III. Motion Simulation and Verification

As the nonlinear dynamic equations are difficult to be solved analytically, the numerical simulation method is adopted to simulate the motion of the AUV and cable system. Based on the simulation scheme introduced in Section III-A, model-based motion simulation is further implemented in Sections III-B and IV. To ensure the accuracy of the simulation results, the modeling method as well as the simulation

$$\mathbf{M} = \begin{bmatrix} 1 & 0 & 0 & 0 & 0 & 0 \\ 0 & 1 & 0 & 0 & V_b\cos\beta & -V_n \\ 0 & 0 & 1 & 0 & -V_b\sin\beta & V_t \\ 0 & 0 & 0 & 1 & V_n\sin\beta - V_t\cos\beta & 0 \\ 0 & 0 & 0 & 0 & -T\cos\beta & 0 \\ 0 & 0 & 0 & 0 & 0 & T \end{bmatrix}$$

$$\mathbf{N} = \begin{bmatrix} -m_c e\frac{V_t}{1+eT} & m_c & 0 & 0 & (m_{cv}V_b - \rho A J_b)\cos\beta & -(m_{cv}V_n - \rho A J_n) \\ e & 0 & 0 & 0 & 0 & 0 \\ 0 & 0 & 0 & 0 & 0 & 1+eT \\ 0 & 0 & 0 & 0 & -(1+eT)\cos\beta & 0 \\ -e\frac{(m_{cv}V_b - \rho A J_b)}{(1+eT)} & 0 & 0 & m_{cv} & (m_{cv}V_n - \rho A J_n)\sin\beta - m_c V_t\cos\beta & 0 \\ -e\frac{(m_{cv}V_n - \rho A J_n)}{(1+eT)} & 0 & m_{cv} & 0 & -(m_{cv}V_b - \rho A J_b)\sin\beta & m_c V_t \end{bmatrix}$$

$$\boldsymbol{q} = \begin{bmatrix} w_c\sin\beta + \frac{1}{2}\rho d\sqrt{1+eT}\pi C_t U_t |U_t| \\ 0 \\ 0 \\ 0 \\ \frac{1}{2}\rho d\sqrt{1+eT}C_n U_b\sqrt{U_n^2+U_b^2} - \rho A\dot{J}_b \\ w_c\cos\beta + \frac{1}{2}\rho d\sqrt{1+eT}C_n U_n\sqrt{U_n^2+U_b^2} - \rho A\dot{J}_n \end{bmatrix}$$

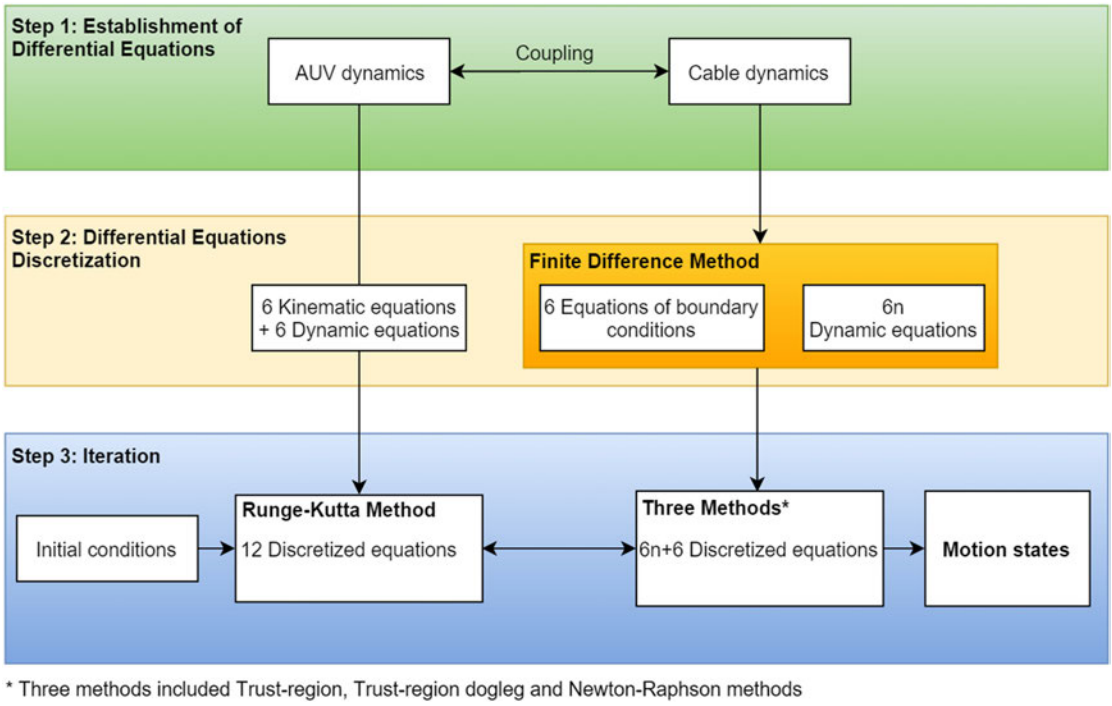

Fig. 3. Flowchart of a numerical simulation scheme.

scheme is verified by comparing the simulation results with the ones published by Feng and Allen [10]; as in their work, the proposed modeling and simulation methods have been validated by experiments.

A. Simulation Scheme

In this article, the model-based simulation process is proceeded as shown in Fig. 3. After the establishment of the respective dynamic equations of the coupled AUV and cable system, the dynamic equations are further discretized for numerical simulation. Thus, different iteration methods could be applied to solve the discretized equations.

As for the cable, the partial differential equations (16) under the boundary conditions (19)–(22) can be solved numerically using FDM. In this method, the cable is considered to be divided into n segments (or nodes) equally, so that the FDM could discretize the cable dynamics both over time (Δt) and cable length (Δs). Note that unlike a typical towed cable, where the length of the cable is fixed in a mission, in our case, the length of the deployed communication cable is increased when the AUV towing the cable moves forward in the water. In this case, the length of each segment of the cable is fixed in the FDM, whereas the number of the total segments of the cable increases as time goes.

Define the centered finite differences at midnodes $s_{j-1/2}$ and at the time instant $t_{i+1/2}$ as

$$\boldsymbol{y}(s_{j-1/2},t_i)=\frac{1}{2}\left[\boldsymbol{y}(s_j,t_i)+y(s_{j-1},t_i)\right]$$

$$\boldsymbol{y}(s_{j-1/2},t_{i+1})=\frac{1}{2}\left[\boldsymbol{y}(s_j,t_{i+1})+y(s_{j-1},t_{i+1})\right]$$

$$\boldsymbol{y}(s_{j-1},t_{i+1/2})=\frac{1}{2}\left[\boldsymbol{y}(s_{j-1},t_i)+y(s_{j-1},t_{i+1})\right]$$

$$\boldsymbol{y}(s_j,t_{i+1/2})=\frac{1}{2}\left[\boldsymbol{y}(s_j,t_i)+y(s_j,t_{i+1})\right]$$

with

$$\Delta s_j=s_j-s_{j-1}$$

$$s_{j-1/2}=\frac{1}{2}\left(s_j+s_{j-1}\right),\quad j=1,2,\ldots,n+1$$

$$t_{i+1/2}=(i+1/2)\,\Delta t,\quad i=0,1,\ldots,k$$

where we assume that the time step Δt is sufficiently small. Applying the governing equations (16) at the points $(s_{j-1/2},t_{i+1/2})$ yields the $6(n+1)$ difference equations as follows [19]:

$$\begin{aligned}&\mathbf{M}(\boldsymbol{y}(s_{j-1/2},t_{i+1}))\frac{\boldsymbol{y}(s_j,t_{i+1})-\boldsymbol{y}(s_{j-1},t_{i+1})}{\Delta s_j}\\&\quad+\mathbf{M}(\boldsymbol{y}(s_{j-1/2},t_i))\frac{\boldsymbol{y}(s_j,t_i)-\boldsymbol{y}(s_{j-1},t_i)}{\Delta s_j}\\&=\mathbf{N}(\boldsymbol{y}(s_j,t_{i+1/2}))\frac{\boldsymbol{y}(s_j,t_{i+1})-\boldsymbol{y}(s_j,t_i)}{\Delta t}\\&\quad+\mathbf{N}(\boldsymbol{y}(s_{j-1},t_{i+1/2}))\frac{\boldsymbol{y}(s_{j-1},t_{i+1})-\boldsymbol{y}(s_{j-1},t_i)}{\Delta t}\\&\quad+\boldsymbol{q}(\boldsymbol{y}(s_{j-1/2},t_{i+1}))+\boldsymbol{q}(y(s_{j-1/2},t_i)).\end{aligned}\tag{23}$$

The above finite difference equation (23) involves $n+1$ cable nodes, and according to (15), there are six motion states used to describe the motion of each cable segment, so there are $6(n+1)$ cable node variables in total. Because the AUV is a rigid body, 12 motion states are used to describe its dynamics. Thus, for the combined AUV and cable system, there are in total $12+6(n+1)$ dynamic equations involved to solve the $12+6(n+1)$ motion states, which are

$$Y=\{y_{1:n+1},(X_v,Y_v,Z_v,\phi,\theta,\psi,u,v,w,p,q,r)\}^T.\tag{24}$$

The initial condition of the system (Y^0) should be provided for further calculation. Then, the previous iteration result (Y^k) will be used

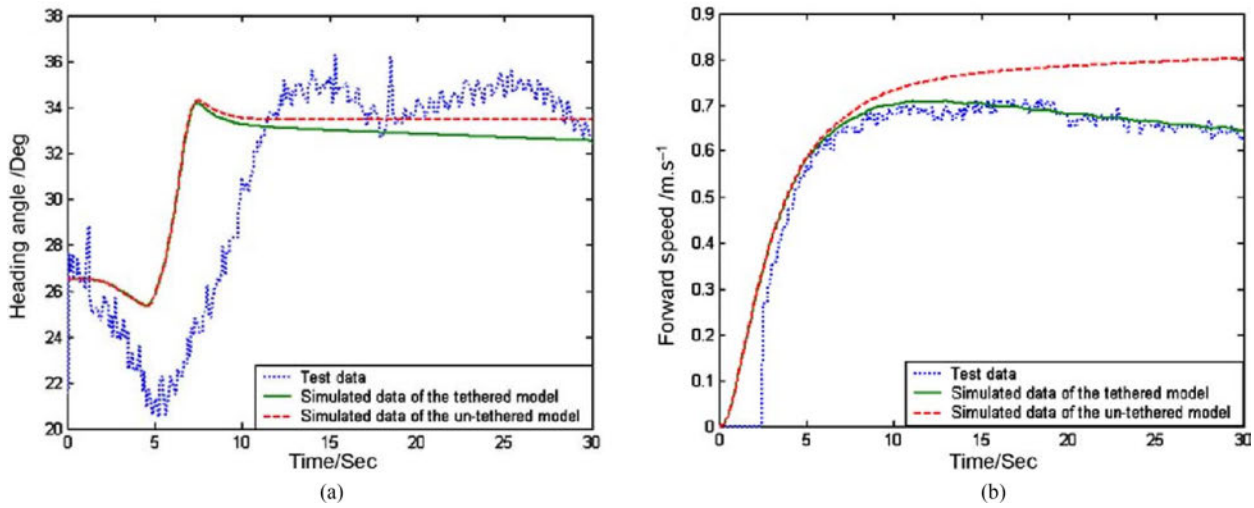

Fig. 4. Validation of the tethered vehicle model [10]. (a) AUV forward speed. (b) AUV heading angle.

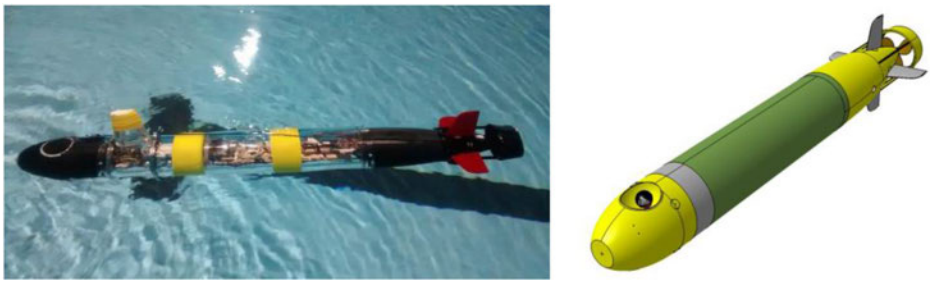

Fig. 5. Configuration of Mullaya AUV [22], [26].

as the initial guess for the next iteration (Y^{k+1}). A converged result is expected for each iteration step [19].

As mentioned in Section I, the TR method will be used to solve the nonlinear finite differential equations in our numerical simulation scheme to obtain more reliable solving results.

B. Modeling Method Verification

To verify the presented modeling method and simulation scheme, study is conducted to compare the simulation results obtained from the presented model in this article with the ones as discussed in Feng and Allen's work [10]. Feng and Allen have validated their AUV and cable coupling model using the field test data that are measured by a set of sensors onboard, as is shown in Fig. 4.

Since the full hydrodynamic model of our Explorer AUV is still under development, due to the availability of an AUV dynamic model, an identical dynamic model of the coupled AUV and cable system has been established with our Mullaya AUV. This vehicle is designed for hydrodynamic testing at AMC (see Fig. 5), whose hydrodynamic coefficients are fully available. Although a different AUV model is used in the simulation from the one (Subzero II AUV) presented in [10], the size and geometry of the two vehicles are similar as is shown in Table I.

For the sake of comparison, a case study has been conducted, which repeats the simulation scenario mentioned in [10]. The cable-tethered AUV moves straightforward for 10 s; then, it decreases its pitch angle by 6 °/s, and after 20 s, the pitch angle remains at –60°. The time series of the vehicle's pitch angle in the case study is defined as follows:

$$\theta(t) = \begin{cases} 0^\circ, & 0 \le t \le 10 \text{ s} \\ -6^\circ \times (t-10), & 10 < t \le 20 \text{ s} \\ -60^\circ, & t > 20 \text{ s}. \end{cases}$$

TABLE I
COMPARISONS OF PHYSICAL PARAMETERS BETWEEN SUBZERO II AUV AND MULLAYA AUV

AUV	Length [m]	Diameter [m]	Mass [kg]	Centre of mass [m]
Subzero II AUV	1	0.1	7	$[0.05,0,0]^T$
Mullaya AUV	1.45	0.177	32	$[0.08,0,0]^T$

The same cable and fluid property parameters are adopted following the study in [10], which are given in Table II. Note that the optical fiber is taken as an inelastic, lightweight, thin, and neutrally buoyant cable.

Fig. 6 presents the simulation comparison results. It can be seen from Fig. 6(a) that there is some slight discrepancy in the configuration of the cable between the two sets of simulation results. This may be due to the larger inertia of Mullaya AUV, which has a larger mass and size than the Subzero II AUV. It is observed in Fig. 6(b) that the results of the cable velocity at the towpoint matches well with each other as well as the

TABLE II
CABLE AND FLUID PARAMETERS

ρ [kg/m^3]	m_c [kg/m]	A [m^2]	m_{cv} [kg/m]	w_c [N/m]	e	C_t	C_n	D [m]
1000	0.0049	4.9e-6	0.0098	0	0	0.01	1	0.0025

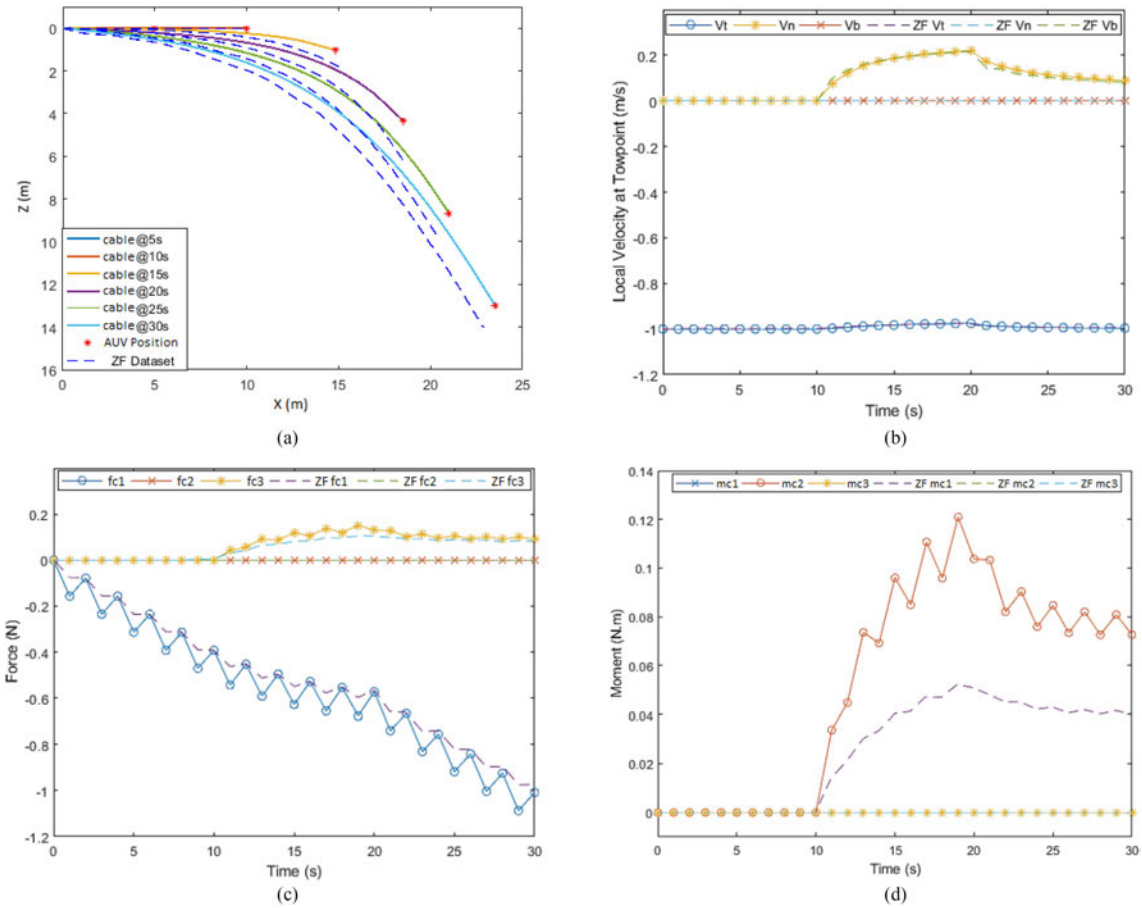

Fig. 6. Simulation results for verification (the prefix "ZF" in the legend denotes the corresponding data obtained from [10]). (a) Cable configuration at different time instants. (b) Cable velocity at the towpoint. (c) Cable-induced force at the towpoint. (d) Cable-induced moment.

value of the cable-induced force at the towpoint as shown in Fig. 6(c). However, an obvious discrepancy in the cable-induced moment acting on the two vehicles is shown in Fig. 6(d), which may be caused by the different distances between the cable towpoint and the center of gravity of the vehicle. There are obvious fluctuations in the cable-induced force in the $\boldsymbol{b}_1$ direction and in the cable-induced moment in the $\boldsymbol{b}_2$ direction, which may be caused by the less stable pitch control of the vehicle during its descending flight. Overall, according to the similarity and the reasonable difference between the compared simulation results, it can be concluded that the accuracy and feasibility of the presented modeling method and simulation scheme in this article is acceptable. Therefore, the model-based simulation can be further implemented for the following motion analysis study.

IV. MOTION ANALYSIS

In this section, we conduct several case studies to investigate the effects of the tethered cable and ocean current on AUV motion using the model-based simulation. Different motion scenarios have been taken into consideration, including straight running, moving in the vertical plane, moving in the horizontal plane, and moving in the 3-D space. Based on the motion analysis, an antitwining maneuvering strategy is further proposed for safe operation of the tethered AUV moving in currents.

There are following assumptions in our simulations.

1) The AUV is moving at equilibrium conditions.
2) Before the vehicle starts to move, the deployed cable length is considered as 0 m. There is no tension acting along the cable. The velocity and rotation angles of each segment along the cable are all equal to 0.
3) A drum is used to release the cable to avoid the generation of tension along the cable.
4) The constant uniform currents are considered in different study cases.
5) The cable tension is estimable or measurable online in real time. Unless the real-time cable tension is available by the vehicle

TABLE III
TENSION AT TOWPOINT VARIED WITH THE CABLE LENGTH

Conditions	Condition 1 (200m)	Condition 2 (500m)	Condition 3 (1000m)
Cable tension at towpoint	7.854 N	19.635 N	51.055 N

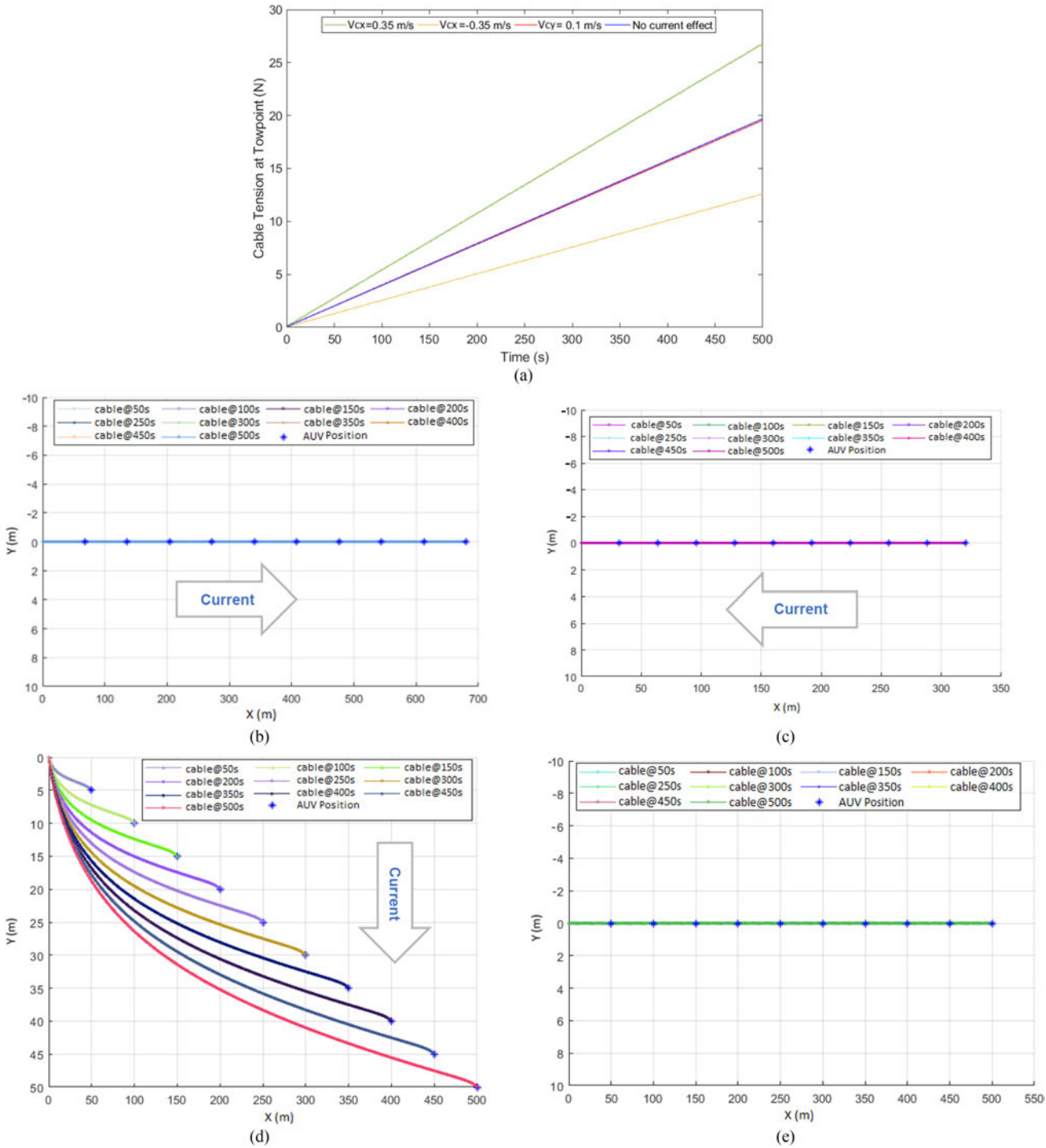

Fig. 7. Current effect on the AUV and cable coupling system in straight running. (a) Cable tension at towpoint in different current conditions. (b) Cable configuration in downstream current. (c) Cable configuration in upstream current. (d) Cable configuration in cross current. (e) Cable configuration in calm water.

control system, the cable tension induced forces and moments (disturbances) acting on the vehicle could be compensated immediately; this will keep the vehicle stay in the desired equilibrium motion status.

A. Straight Running

In this case, the Mullaya AUV starts at the origin of the inertial frame and moves straightforward in the horizontal plane at the speed of 1 m/s in calm water, with all the attitude angles equal to 0. The change in the cable tension at the vehicle-side towpoint is observed as the cable length increases when the AUV moves forward. The cable tensions in three conditions are compared when the cable length grows up to 200, 500, and 1000 m, respectively. The results are presented in Table III. It is obvious that as the length of the deployed cable increases, the cable tension acting at the towpoint will increase. When tethered by a 1000-m cable, it will take the vehicle an addition of at least 51.055 N propulsion force to compensate the cable effect and maintain the desired forward speed. So, special attention should be paid to the effect of cable tension when the vehicle is tethered by a cable in its mission.

Furthermore, the ocean current effect on the straight motion of the coupled AUV and cable system is studied. In this study, four kinds of constant current conditions are considered: downstream with current velocity of $V_{cx} = 0.35$ m/s, upstream with current velocity of $V_{cx} = -0.35$ m/s, cross current with velocity of $V_{cy} = -0.1$ m/s, and no current.

The time series of the cable tension at the towpoint and the cable configuration for each current condition are presented in Fig. 7. The cable tension at the towpoint is highest when the vehicle is moving in the upstream current. In this case, the vehicle's absolute velocity is increased by the current, so in the given time range of 500 s, the longest cable is deployed into the water. As is found from the previous study, longer deployed cable can generate larger tension at the towpoint of the vehicle. On the contrary, the cable tension is lowest when the vehicle is moving against the current in a 500-s run. Since the slight cross current does not dramatically change the length of the deployed cable within 500 s, the cable tension in the cross current is similar to the one in calm water. It is also observed that the vehicle and the cable are pushed to the starboard side in the cross current with an obvious displacement in the positive $\boldsymbol{i}_2$ direction in Fig. 7(d).

B. Motion in the Vertical Plane

In this study, the current effect on the AUV and cable coupling system is investigated when the AUV maneuvers in the vertical plane. In the simulation, the vehicle starts at the origin of the inertial frame with the forward speed of 1 m/s while its pitch angle θ varies as shown in Fig. 8.

The simulation results for the tethered AUV moving with and without current disturbance are, respectively, given in Fig. 9. Both the variation in the cable tension at the towpoint and the configuration of the cable for the two cases are compared. In this study, the ocean current in the positive $\boldsymbol{i}_1$ direction is considered with a constant velocity of 0.5 m/s at all the depths while the vehicle moves downstream in the $\{\boldsymbol{i}_1, \boldsymbol{i}_3\}$ plane. As the vehicle can hardly get tangled in the cable if moving against the current, here we intend to study the worst case that may cause tangling.

From the comparison between Fig. 9(a) and (c), it can be found that the downstream current changes the configuration of the cable. As the forward speed of the AUV and cable system is increased by the current, the deployed cable length is longer than the one without current disturbance. Since the current carries the vehicle and the cable together to move forward, although moving in the downstream current, it is still not easy for the vehicle to get tangled by the cable as long as it is moving forward. As is shown in Fig. 9(b) and (d), the overall cable tension increases when there is current disturbance, whereas the cable tension at the towpoint decreases at the time ranges from 100 to 120 s and from 160 to 180 s for both cases. This is because the cable tension at the towpoint increases when the vehicle is traveling in one direction, like at a fixed pitch angle, whereas the cable tension will decrease to some extent when the vehicle is changing to travel in an opposite direction, such as changing its pitch angle to an opposite direction. Thus, when deploying the AUV and cable coupling system, one can design the maneuvering form of the vehicle to control the cable tension at the towpoint and make it within an acceptable range.

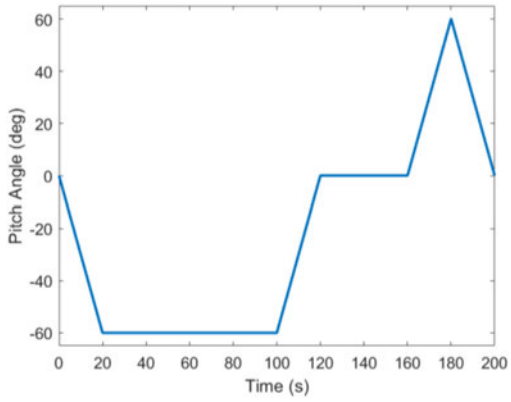

Fig. 8. Variation in vehicle pitch angles.

C. Motion in the Horizontal Plane

Next, the motion of the coupled AUV and cable system in the horizontal plane is studied. Here, we consider two kinds of motion cases when the vehicle moves in the horizontal plane. In the first case, the vehicle starts at the origin of the inertial frame and runs in a zig-zag pattern without current disturbance. The forward speed of the vehicle is set at 1 m/s while the variation in the heading angle ψ is defined as shown in Fig. 10(a).

The variation in AUV trajectory and the configuration of the cable is shown in Fig. 10(b). It can be found that both the vehicle trajectory and the configuration of the cable appear like sinusoids. However, the period of the vehicle trajectory looks constant, the period of the cable configuration curve seems increasing over time.

In the second case, the vehicle makes a circle in the horizontal plane in current. In the simulation, the current in the negative $\boldsymbol{i}_1$ direction is considered with a constant velocity of 0.1 m/s. The vehicle starts from the origin of the inertial frame while the variation in the vehicle heading angle is defined as shown in Fig. 11(a).

The variation in AUV trajectory and the configuration of the cable is shown in Fig. 11(b). It shows that the vehicle has the risk of getting tangled by the cable when it returns to the start point after making a circle under the disturbance of current. So, special attention should be paid to this case when recovering a tethered AUV. A possible solution is that the vehicle turns to the port side at certain angle at the beginning and then turns to the starboard side to complete the circle when making a right turn, as is shown in Fig. 12(a). Performing in this form, the cable will not drift over the area where the vehicle will pass through for returning [see Fig. 12(b)].

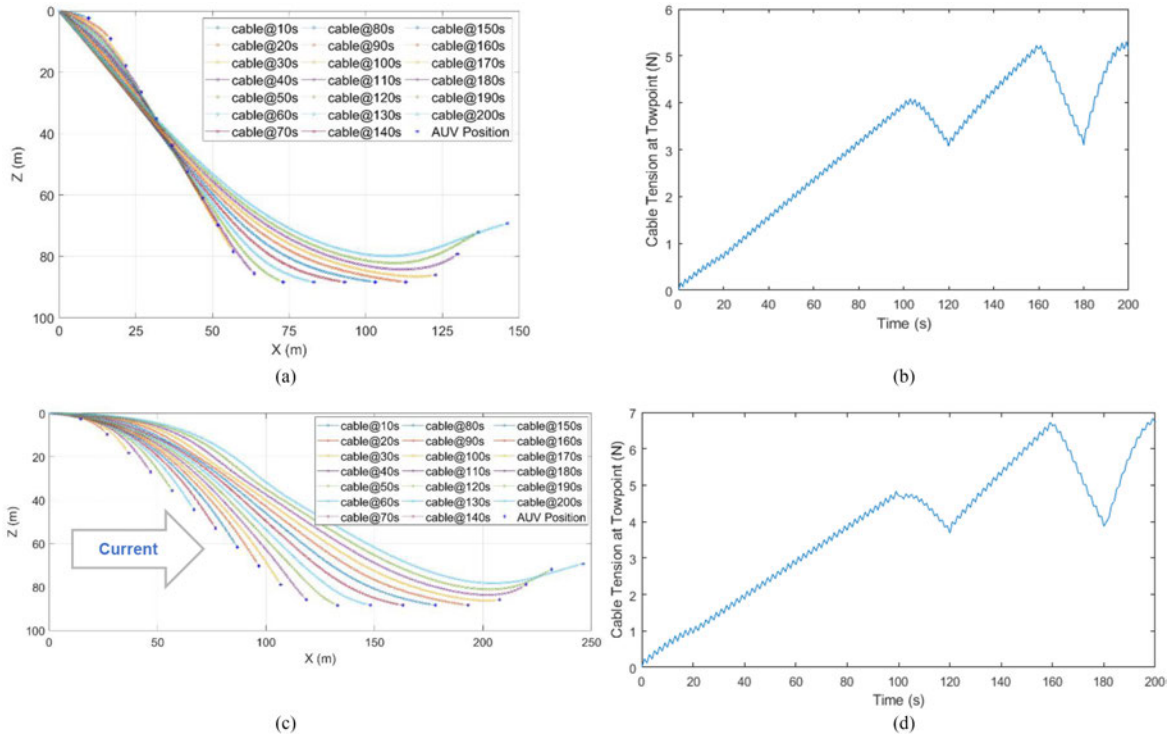

Fig. 9. Current effect on the AUV and cable coupling system when manoeuvering in the vertical plane. (a) Cable configuration in calm water. (b) Cable tension in calm water. (c) Cable configuration in current. (d) Cable tension in current.

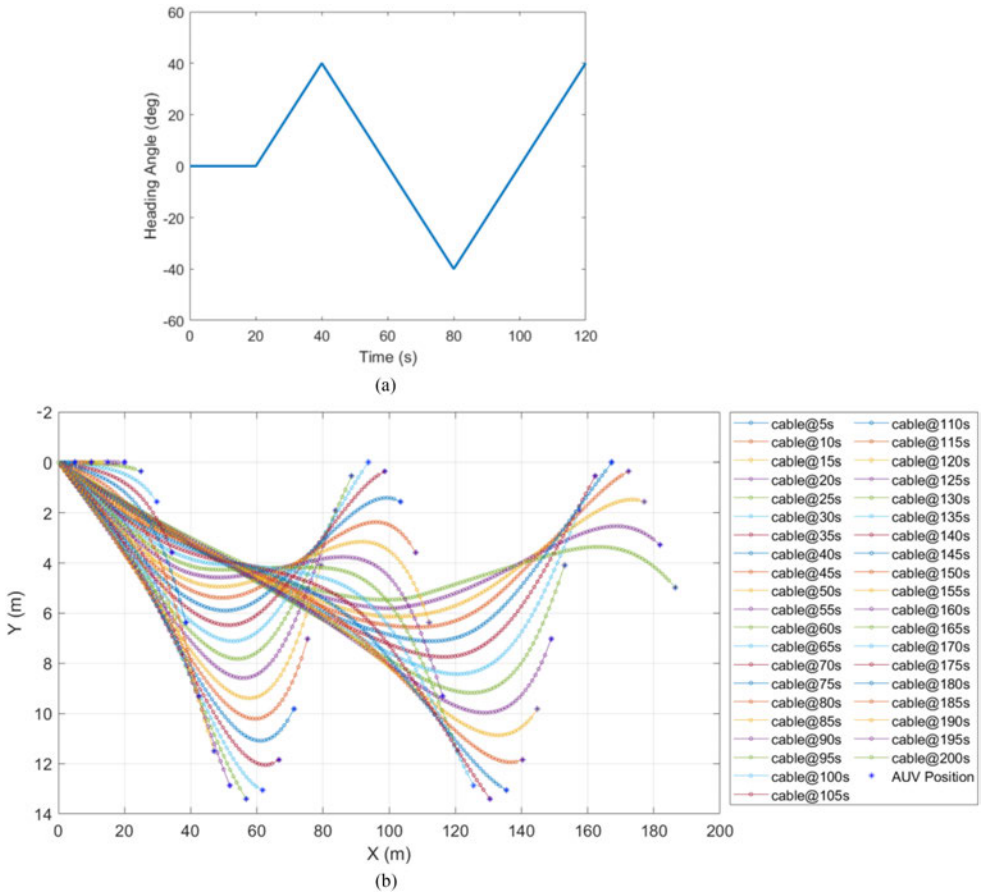

Fig. 10. Simulation input and result of zig-zag motion in the horizontal plane without current disturbance. (a) Variation in vehicle heading angle. (b) AUV trajectory and cable configuration.

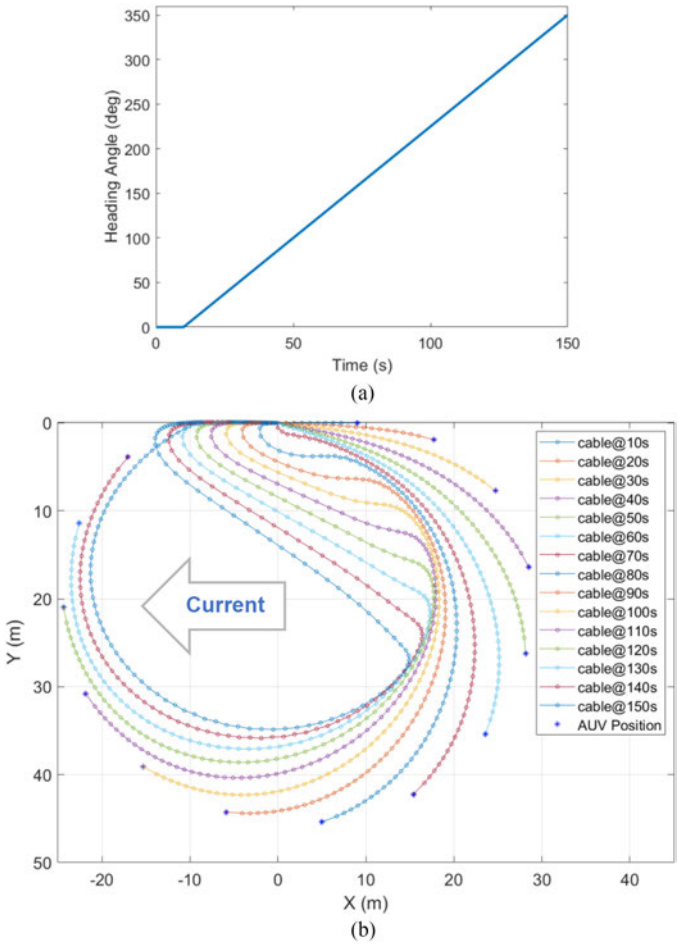

Fig. 11. Simulation input and result of horizontal circling motion without antitwining maneuvering strategy. (a) Variation in vehicle heading angle. (b) AUV trajectory and cable configuration.

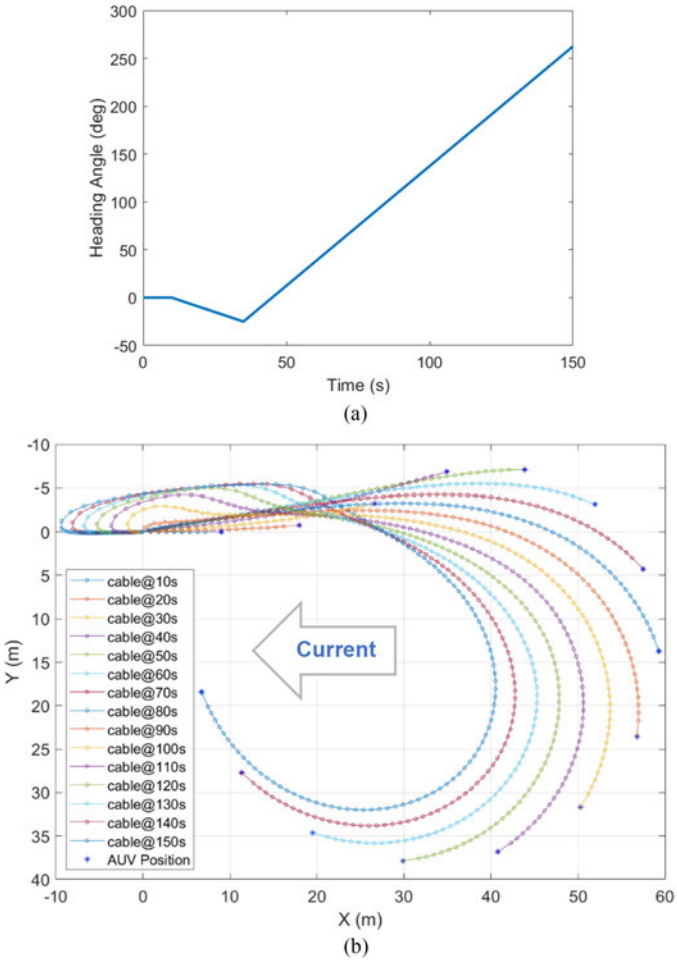

Fig. 12. Simulation input and result of horizontal circling motion with the antitwining maneuvering strategy. (a) Variation in vehicle heading angle. (b) AUV trajectory and cable configuration.

D. Motion in 3-D Space

In this section, the motion of the cable tethered AUV system in 3-D space is presented. In the simulation, the vehicle is commanded to perform downward spiral motion. The vehicle starts from the origin of the inertial frame. The forward speed of the vehicle is set at 1 m/s, and the pitch angle θ is fixed at 10°, whereas the variation in the heading angle ψ is defined as shown in Fig. 13(a).

The simulation results for the tethered AUV moving in two different current conditions are given in Fig. 13(b) and (c), respectively. In Fig. 13(b), the current in the positive $\boldsymbol{i}_2$ direction is considered with a constant velocity of 0.05 m/s at all the depths, and the current in the opposite direction is also with a constant velocity of 0.05 m/s as shown in Fig. 13(c). It is found that the diameter of the turning circle of the cable will increase when the vehicle starts spiraling in downstream current, whereas the diameter of the turning circle of the cable will decrease when the vehicle starts spiraling in upstream current. It also appears that both the vehicle trajectory and the cable profile drift along the current direction as a whole, so the vehicle is hardly to get tangled by the cable in both current conditions. Moreover, at the given pitch angle and heading rate of the spiral motion, the cable will not get tangled by itself in the uniform current.

V. Discussion on Simulation Results

In the previous motion analysis, both the variation in the cable tension at the towpoint and the configuration of the cable are investigated. It is found that the cable tension causes the extra drag on AUV motion, which will affect the motion behavior and endurance capacity of the vehicle, whereas the variation in cable configuration may get the vehicle tangled especially under the disturbance of ocean current. The above-mentioned two issues will be further discussed in this section based on the simulation results in Section III.

A. Cable Tension at the Towpoint

For a tethered AUV, it will take the vehicle additional propulsion to compensate the drag caused by the cable and maintain the desired forward speed. In general, the cable drag will increase as the length of the cable increases, so the maximum affordable cable length for an AUV will depend on the propulsion capability and the power capacity of the vehicle. However, if the proper maneuvering strategy is adopted, one can control the cable tension to make it within an acceptable range, for example by switching the orientation of the vehicle from time to time. Since the uniform current carries the AUV and cable coupling system as a whole to move forward, it will cause less effect on the cable

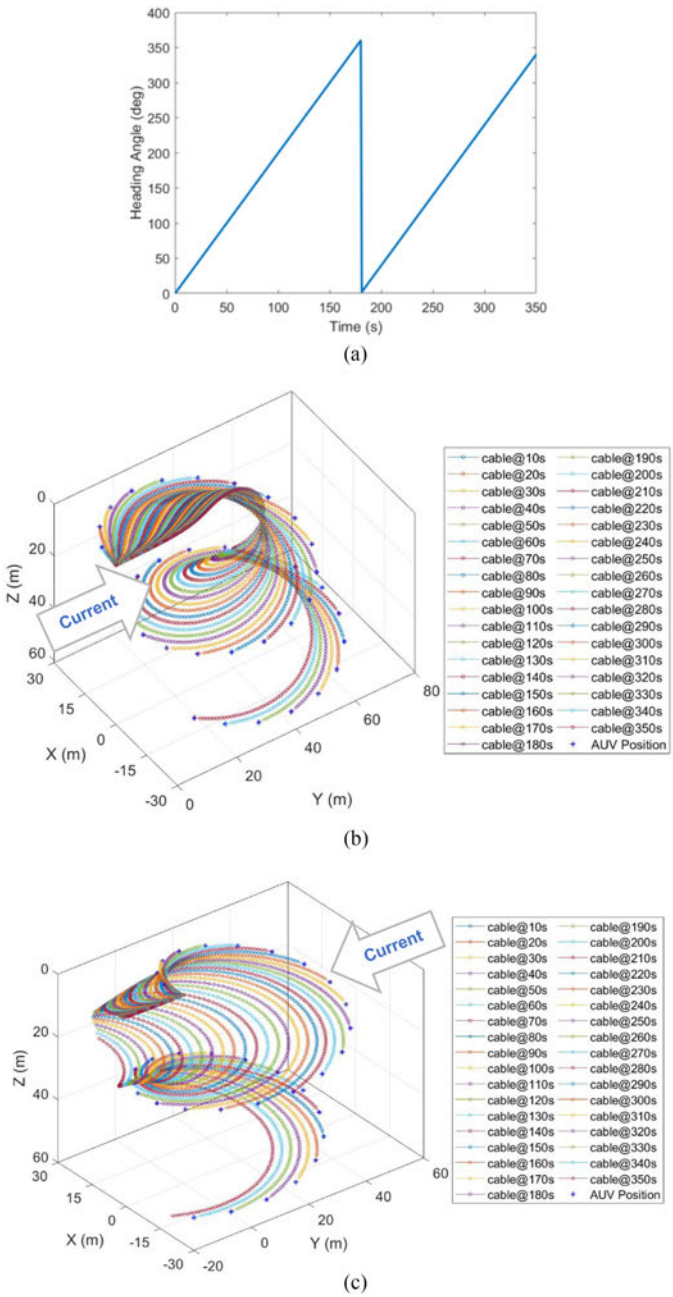

Fig. 13. Simulation input and result of spiral motion in currents. (a) Variation in vehicle heading. (b) AUV trajectory and cable configuration starting with downstream current. (c) AUV trajectory and cable configuration starting with upstream current.

tension. However, in the real world, the ocean environment is much more complicated with unsteady nonuniform current components. In this case, the current effect on the AUV and cable coupling system will be more complex, so further studies should be conducted to investigate this issue.

B. Antitwining Manoeuvering Strategy

With regard to the twining issue of the coupled system, as long as the tethered AUV moves forward, it will be difficult for the vehicle to get tangled by the cable if there is no current. However, the motion of the AUV and the ocean current affects the cable configuration heavily. It is found that the diameter of the turning circle of the cable will vary when the vehicle starts spiraling in different current conditions, such as in downstream or upstream current. Generally, as the cable is neutrally buoyant and has less inertia, it is much easier for the deployed cable to drift along the current. If the current environment is too complicated, the vehicle will run into high risk of twining with the cable.

In the given current environment, if adopting a proper antitwining maneuvering strategy, it will help the vehicle to escape from twining with the cable. Taking the circling motion for example, it is better for the vehicle to navigate against current to make the whole cable body move backward. Besides, the vehicle should start to turn to certain direction for a while if intending to make a circle in the opposite direction; by doing this, the cable will leave the entry area when the vehicle completes the circle and returns to the start point. Again, more thorough antitwining maneuvering strategies should be studied when the vehicle is moving in more dynamic ocean environments.

VI. Conclusion

This article presented the mathematical model of a cable-tethered AUV system as well as the numerical simulation scheme for the coupled motion analysis. In our study, the TR method was used to solve the partial differential equations of cable dynamics as it could provide more accurate results than other methods. The presented model-based simulation scheme was verified by comparing the simulation results with the ones in the existing literature, in which the adopted modeling and simulation methods were validated by the experimental results. Furthermore, a series of simulations were conducted to analyze the motion interaction in the coupled AUV and cable system, especially under the disturbance of ocean currents. In our simulation, different motion cases were studied as the vehicle moves in 1-D, 2-D, and 3-D spaces, respectively. The variation in the cable tension at the towpoint and the configuration of the cable were investigated in different current conditions. We found that the cable tension caused the extra drag on AUV motion, which would affect the motion behavior and endurance capacity of the vehicle, while the variation in the configuration of the cable may get the vehicle tangled especially when the coupled system moves in currents. These two issues were both well discussed in details at the end of this article.

In our current work, we discussed the equilibrium motion states of the vehicle in our simulations, whereas the propulsion dynamics was not considered in the vehicle dynamic model. However, including the propulsion dynamics as well as the consideration of the dynamic level of cable effects on vehicle dynamics will make the simulation more actual, which should be considered in our future work. Besides, only the uniform current was considered for the case studies in this article, whereas in the real world, the ocean environment is much more complicated with unsteady nonuniform components, in which case, the current effect on the cable-tethered AUV should be further investigated in our future study to provide effective and practical guidelines for the safe operation of the AUV and cable coupling system in the field.

Acknowledgment

The authors would like to express their great gratitude to Dr. R. Allen from the University of Southampton, Southampton, U.K., and Dr. Z. Feng from Shanghai Jiao Tong University, Shanghai, China, for their generous support on this study. They would also like to thank the reviewers for their valuable comments, which make this article more presentable. K. Chan and C. K. H. Chin would like to thank the Defence Science and Technology Group for the loan of the Mullaya AUV.

REFERENCES

[1] D. W. Caress *et al.*, "High-resolution multibeam, sidescan, and subbottom surveys using the MBARI AUV D. Allan B.," in *Marine Habitat Mapping Technology for Alaska*. Fairbanks, AK, USA: Alaska Sea Grant Coll. Program, Univ. Alaska Fairbanks, 2008, pp. 47–69.

[2] N. A. Cruz and A. C. Matos, "Adaptive sampling of thermoclines with autonomous underwater vehicles," in *Proc. MTS/IEEE OCEANS Conf.*, 2010, pp. 1–6, doi: 10.1109/OCEANS.2010.5663903.

[3] Y. Zhang *et al.*, "A peak-capture algorithm used on an autonomous underwater vehicle in the 2010 Gulf of Mexico oil spill response scientific survey," *J. Field Robot.*, vol. 28, no. 4, pp. 484–496, 2011.

[4] D. P. Williams, "On optimal AUV track-spacing for underwater mine detection," in *Proc. IEEE Int. Conf. Robot. Autom.*, 2010, pp. 4755–4762.

[5] L. Paull, S. Saeedi, M. Seto, and H. Li, "Sensor-driven online coverage planning for autonomous underwater vehicles," *IEEE/ASME Trans. Mechatronics*, vol. 18, no. 6, pp. 1827–1838, Dec. 2013.

[6] M. Stojanovic, "Recent advances in high-speed underwater acoustic communications," *IEEE J. Ocean Eng.*, vol. 21, no. 2, pp. 125–136, Apr. 1996.

[7] M. Chitre, S. Shahabudeen, and M. Stojanovic, "Underwater acoustic communications and networking: Recent advances and future challenges," *Mar. Technol. Soc. J.*, vol. 42, no. 1, pp. 103–116, 2008.

[8] T. C. Wu, Y. C. Chi, H. Y. Wang, C. T. Tsai, and G. R. Lin, "Blue laser diode enables underwater communication at 12.4 Gbps," *Sci. Rep.*, vol. 7, no. 40480, pp. 1–10, 2017.

[9] F. Hanson and S. Radic, "High bandwidth underwater optical communication," *Appl. Opt.*, vol. 47, no. 2, pp. 277–283, 2008.

[10] Z. Feng and R. Allen, "Evaluation of the effects of the communication cable on the dynamics of an underwater flight vehicle," *Ocean Eng.*, vol. 31, no. 2004, pp. 1019–1035, 2004.

[11] T. V. Mai, H. S. Choi, J. Kang, D. H. Ji, and S. K. Jeong, "A study on hovering motion of the underwater vehicle with umbilical cable," *Ocean Eng.*, vol. 135, pp. 137–157, 2017.

[12] Australian Maritime College. 2017. [Online]. Available: https://www.amcsearch.com.au/autonomous-underwater-vehicles-auvs

[13] M. J. Casarella and M. Parsons, "Cable systems under hydrodynamic loading," *Mar. Technol. Soc. J.*, vol. 4, no. 4, pp. 27–44, 1970.

[14] D. A. Yoerger, M. A. Grosenbaugh, and M. S. Triantafyllou, "Drag forces and flow induced vibrations of a long vertical tow cable-part1: Steady-state towing conditions," *J. Offshore Mech. Arct. Eng.*, vol. 19, no. 3, pp. 117–127, 1991.

[15] F. S. Hover and D. R. Yoerger, "Identification of low-order dynamic models for deeply towed underwater vehicle systems," *Int. J. Offshore Polar*, vol. 2, pp. 38–45, 1992.

[16] Y. T. Chai and K. S. Varyani, "Three dimensional lump mass formulation of a catenary riser with bending, torsion and irregular seabed interaction effect," *Ocean Eng.*, vol. 29, pp. 1503–1525, 2002.

[17] Q. Li, H. Xu, Q. Zhang, X. Wang, and Z. Li, "Dynamics simulation of remotely operated vehicle-fiber optic micro cable system," in *Proc. 7th World Congr. Intell. Control Autom.*, 2008, pp. 2311–2314.

[18] C. M. Ablow and S. Schechter, "Numerical simulation of undersea cable dynamics," *Ocean Eng.*, vol. 10, no. 6, pp. 443–457, 1983.

[19] F. Milinazzo, M. Wilkie, and S. A. Latchman, "An efficient algorithm for simulating the dynamics of towed cable systems," *Ocean Eng.*, vol. 14, no. 6, pp. 513–526, 1987.

[20] The MathWorks, Inc., "Equation Solving Algorithms," 2018. [Online]. Available: http://au.mathworks.com/help/optim/ug/equation-solving-algorithms.html

[21] T. I. Fossen, *Guidance and Control of Ocean Vehicles*. New York, NY, USA: Wiley, 1994.

[22] B. J. Fitzgerald, "Prediction of hydrodynamic and manoeuvring characteristics of the AUV Mullaya through CFD and experimental work," Bachelor project, Australian Marit. Coll, Newnham TAS, Australia, 2009.

[23] B. Namani, "Investigation of hydrodynamic characteristics of propulsion system for Mullaya AUV with respect to angle of fins," Master thesis, Nat. Centre Maritime Eng. Hydrodynamics, Australian Marit. Coll, Newnham TAS, Australia, 2019.

[24] S. Fan, B. Li, W. Xu, and Y. Xu, "Impact of current disturbances on AUV docking: model-based motion prediction and countering approaches," *IEEE J. Ocean Eng.*, vol. 43, no. 4, pp. 888–904, Oct. 2018.

[25] C. A. Woolsey, "Vehicle dynamics in currents," , Virginia Centre Auton. Syst., Virginia Polytech. Inst. State Univ. (Virginia Tech), Blacksburg, VA, USA, Tech. Rep. VaCAS-2011-01, Sep. 2011.

[26] W. Ariza Ramirez, "Gaussian processes applied to system identification, navigation and control of underwater vehicles," Ph.D. dissertation, Nat. Centre Maritime Eng. Hydrodynamics, Australian Marit. Coll., Newnham TAS, Australia, 2019.

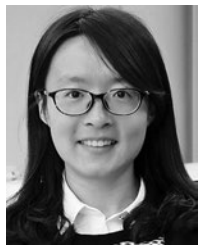

Shuangshuang Fan received the B.E. degree in mechanical engineering from Shandong University, Jinan, China, in 2008 and the Ph.D. degree in mechatronics from Zhejiang University, Hangzhou, China, in 2013.

From October 2013 to October 2014, she was a Research Engineer with the Institute of Shanghai Aerospace Control Technology, Shanghai, China. She was with the Acoustic Signal Processing Lab, Zhejiang University, as a Postdoctoral Researcher from November 2014 to April 2017. From May 2017 to July 2019, she was a Lecturer with the Australian Maritime College, University of Tasmania, Launceston, TAS, Australia. She is currently an Associate Professor with the School of Marine Sciences, Sun Yat-sen University, Zhuhai, China. She is also an Adjunct Professor with the Department of Ocean and Naval Architectural Engineering, Memorial University of Newfoundland, St. John's, NL, Canada. Her research interests include the navigation, control, and path planning of underwater vehicles in dynamic environments.

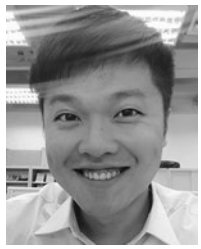

Kamchau Chan received the B.E degree in naval architecture from the Australian Maritime College, University of Tasmania, Launceston, TAS, Australia, in 2019.

He is currently a Charter Engineer in the marine industry. His work scope is mostly to provide professional advice and engineering solutions to solve marine investigation problems, including using autonomous underwater vehicles.

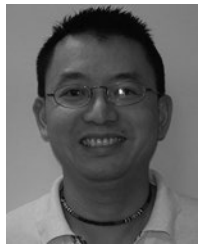

Christopher K. H. Chin received the B.App.Sci (Hons.) degree in mathematics and the Ph.D. degree in mathematics from RMIT University, Melbourne, VIC, Australia, in 1997 and 2003, respectively.

He was appointed as a Lecturer with the Australian Maritime College (AMC) in 2014. He has held several roles over the past few years including a First Year Coordinator of the Maritime Engineering degree, the Deputy Director (Students and Education) with the National Centre for Maritime Engineering and Hydrodynamics, AMC, and the Deputy Associate Dean of Learning and Teaching with the College of Sciences and Engineering, University of Tasmania. He is currently a Senior Lecturer with AMC and is the Course Leader for the Maritime Engineering program. His research interests include engineering education, renewables, autonomous underwater vehicles, and path planning.